A black body absorber from vertically aligned single-walled carbon nanotubes

Kohei Mizuno[a], Juntaro Ishii[b], Hideo Kishida[c], Yuhei Hayamizu[a], Satoshi Yasuda[a], Don N. Futaba[a], Motoo Yumura[a], and Kenji Hata[a,1]

[a]Research Center for Advanced Carbon Materials, National Institute of Advanced Industrial Science and Technology, Tsukuba, Ibaraki 305-8565, Japan; [b]National Metrology Institute of Japan, National Institute of Advanced Industrial Science and Technology, Tsukuba, Ibaraki 305-8563, Japan; and [c]Department of Applied Physics, Nagoya University, Chikusa-ku, Nagoya 464-8603, Japan

Communicated by Sumio Iijima, Meijo University, Nagoya, Japan, January 29, 2009 (received for review October 19, 2008)

Among all known materials, we found that a forest of vertically aligned single-walled carbon nanotubes behaves most similarly to a black body, a theoretical material that absorbs all incident light. A requirement for an object to behave as a black body is to perfectly absorb light of all wavelengths. This important feature has not been observed for real materials because materials intrinsically have specific absorption bands because of their structure and composition. We found a material that can absorb light almost perfectly across a very wide spectral range (0.2–200 μm). We attribute this black body behavior to stem from the sparseness and imperfect alignment of the vertical single-walled carbon nanotubes.

absorbance | emissivity | reflectance

A black body is a theoretical object that absorbs all light that falls on it, because no light is transmitted or reflected (1). As a result, it appears perfectly black at room temperature and is the most efficient thermal absorber and emitter because any object at thermal equilibrium will emit the same amount of light as it absorbs at every wavelength. The radiation spectrum of a black body is determined solely by the temperature and not by the material, properties, and structure. These features, as an ideal source to emit or absorb radiation, make the black body valuable for many applications. For example, because the black body efficiently converts light to heat, it has great importance to solar energy collectors (2–5) and infrared thermal detectors, such as pyroelectric sensors (6–8). As a perfect emitter of radiation, a hot material with black body behavior would create an efficient infrared heater and would be valuable for heat liberation (9), particularly in space or in a vacuum where convective cooling is negligible.

A requirement for an object to behave as a black body is that it perfectly absorbs light of all wavelengths; yet, in reality, black bodies do not exist. Emissivity is a measure of how similar an object is to a black body and is defined as the ratio of the energy radiated by that object and by a black body. Therefore, a black body would possess emissivity of unity for all wavelengths. This important feature has not been observed for real materials because materials intrinsically have specific absorption bands because of their structure and composition, and thus, the emissivity of any real object is less than unity and is wavelength dependent.

A good approximation of a black body is a cavity; however, this structure limits its utility. A material exhibiting black body behavior would solve this structural limitation and increase its practical usefulness. Hence, various processes and materials have been developed to blacken the surface by chemical treatment (10, 11), plating (4–6), and painting (8). Despite these efforts, emissivities for black coatings (Astro Black), chemically treated black surfaces (Hino Black), and microscale needle-like structure of nickel-phosphorus alloy (Anritsu Black) can be as high as 0.96 at 5–9 μm but decreases notably at >9 μm (Fig. 1) (12). Carbon is a good absorber because of the π-band's optical transitions, and it is thus used in many conventional black materials such as carbon black and graphite (13). Yet the emissivity is limited to 0.8–0.85 because of the moderate reflection at the air–dielectric interface (14). One interesting approach to overcome this limit is to use nanostructures (15–17), especially vertically aligned carbon nanotubes (forest) (3, 15). Recently, Ajayan et al. (18) measured the reflectance of forests by 4 visible lasers at 4 specific wavelengths in the range of 457–633 nm and revealed the extremely low reflectance (0.045%) of the forest. This result shows that a forest absorbs light very efficiently at some specific wavelengths.

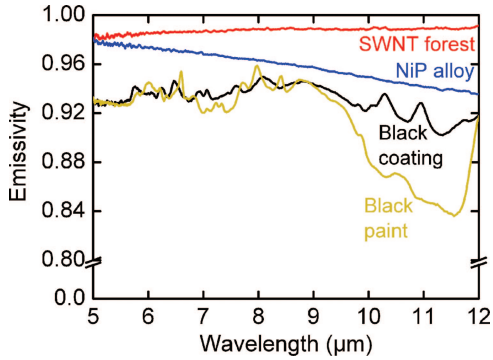

Fig. 1. Normal spectral emissivity of SWNT forest (red line) and commercially available black surfaces that are denoted as NiP alloy (blue), black coating (black), and black paint (yellow). Spectrum data of the black surfaces from ref. 12 with the permission of the author.

Here, we report that among all known materials, a forest of vertically aligned single-walled carbon nanotubes (SWNTs) behaves most similarly to a black body. Specifically, from optical studies, we revealed that a SWNT forest possesses a nearly constant and near-unity emissivity (absorptivity) of 0.98–0.99 across a wide spectral range from UV (200 nm) to far infrared (200 μm). We speculate that this important black body behavior originates from the homogeneous sparseness and alignment of the SWNTs within the forest.

Results and Discussion

As observed by the naked eye, the SWNT forest appears to be very black as shown by a picture of an 8-in silicon wafer in Fig. 2*A*. SEM images of the forest from an angled view show the uniformly flat top surface (Fig. 2*B*) and the nanotube vertical alignment [Fig. 2 *C* (top) and *D* (side)].

Author contributions: K.M., J.I., H.K., M.Y., and K.H. designed research; K.M., J.I., H.K., S.Y., D.N.F., and K.H. performed research; K.M., J.I., H.K., Y.H., and K.H. analyzed data; and K.M., D.N.F., and K.H. wrote the paper.

The authors declare no conflict of interest.

[1]To whom correspondence should be addressed. E-mail: kenji-hata@aist.go.jp.

This article contains supporting information online at www.pnas.org/cgi/content/full/0900155106/DCSupplemental.

www.pnas.org/cgi/doi/10.1073/pnas.0900155106

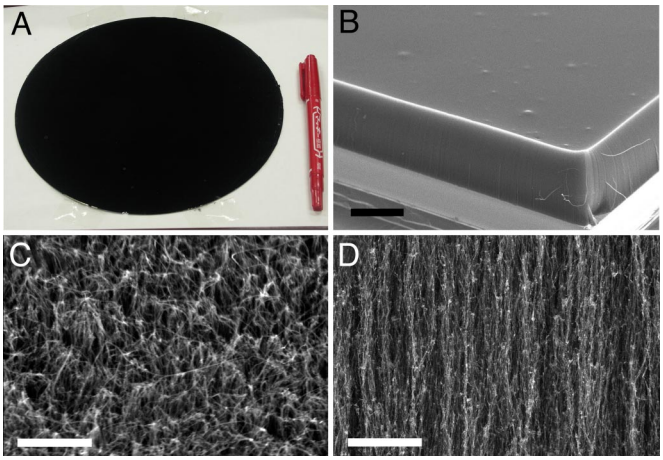

Fig. 2. Microscopic structure of SWNT forest. (*A*) SWNT forest grown on an 8-in silicon wafer. (*B*) SEM image of SWNT forest vertically standing on a silicon substrate. (Scale bar, 0.5 mm.) (*C*) SEM image showing top surface of SWNT forest. (Scale bar, 0.5 μm.) (*D*) SEM image showing side surface of SWNT forest. (Scale bar, 5 μm.)

The emissivity spectrum of a SWNT forest (height: 460 μm, density: 0.07 g cm^{-3}) in thermal equilibrium at 373 K reveals that the SWNT forest has a remarkably high emissivity of 0.98–0.99 in the spectral range of 5–12 μm (Fig. 1). This emissivity is significantly higher than conventional black materials and represents the highest ever reported to the best of our knowledge. More importantly, in contrast to conventional black materials, the emissivity of the SWNT forest is nearly wavelength independent (standard deviation 0.003) across the whole measured spectral range. To examine the structural requirements for high emissivity, we carried out a number of distinct experiments. First, investigation of forests with heights spanning 2–460 μm showed an emissivity of >0.97 even for a 2-μm-tall forest and an emissivity of >0.98 for forests taller than 50 μm [see also supporting information (SI) Fig. S1]. Second, emissivity examination of forest densities ranging from 0.029 to 0.084 g cm^{-3} (Fig. 3*A*) showed no obvious trends. However, by combining these results, a clear trend emerged where the emissivity increased with increased area mass density (defined by height × density) (Fig. 3*B*). The emissivity increased to 0.987, >2.33 mg cm^{-2}, which corresponds to 3.1 × 10^4 layers of graphene sheet per unit area.

Although the wavelength-independent ≈0.98 emissivity strongly implies that the nanotube forest resembles a black body, ideally, the emissivity needs to be unity across an extremely large spectral range; however, the experimental range was rather limited (5–12 μm). This experimental limitation was addressed by indirectly estimating the emissivity by measuring the reflectivity and by using Kirchhoff's law, e.g., the emissivity of an object equals to its absorptivity, and the sum of reflectivity, transmissivity, and absorptivity equals 1 in thermal equilibrium. Therefore, provided zero transmissivity, emissivity is equal to 1− reflectivity. To cover an extensively wide spectral range from UV to far infrared, the optical reflectance and transmittance of the SWNT forests was studied by 3 independent optical systems (see also Table S1). In the mid-to-far IR region, the transmittance of a Si substrate with a SWNT forest (600-μm thickness) dramatically decreased <0.002 compared with that of a bare Si substrate (0.2–0.5). For the other spectral regions, the transmittance was below the detection limit, and this near-zero transmittance confirms that the emissivity equals 1− reflectivity.

Significantly, the reflectance of the nanotube forests (300- to 500-μm height) was not only extremely low at 0.01–0.02 but also

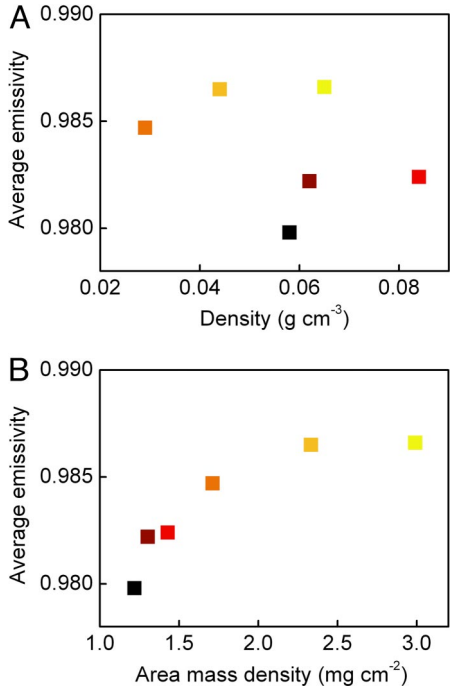

Fig. 3. Average emissivity as a function of bulk density (*A*) and of area mass density (*B*) of SWNT forest, respectively.

unvarying across the entire spectral range (Fig. 4). Hemispherical (specular + diffuse) reflectance in the UV-to-near IR and the near-to-mid IR range was extremely low as 0.01–0.02 and was wavelength independent (Fig. 4 *A* and *B*).

In the mid-to-far IR range, only the specular reflectance is measurable because a reliable integrating sphere for spectral range does not exist. As such, in this range, not the hemispherical but the specular reflectance was measured. The measured specular reflectance was <0.002 and wavelength independent. These results strongly suggest that the unvarying low reflectance characteristic also extends to this spectral range (Fig. 4*C*). It should be noted that the diffuse reflectance may be much larger for the spectral region >20 μm, and we expect that this research will encourage future efforts to address this important point.

The reflectance spectra show small irregularities and mild monotonic increases with wavelength that are likely because of experimental uncertainties in the reference and the integrating sphere and detection limits of the apparatus. These low and wavelength-independent hemispherical reflectance measurements of <0.02 in the UV-to-mid IR are consistent with the high and wavelength-independent emissivity measurements of >0.98. The high and uniform emissivity, the good match between the reflectance and emissivity measurements, and the low and constant reflectance over a very wide wavelength range strongly suggests that the SWNT forest is almost identical to an ideal black body.

To gain deeper insights into the origin of the nanotube forest black body behavior, we carried out emissivity measurements on several distinct nanotube structures that revealed the importance of the structure. Three different SWNT forms were made from a nanotube forest: a roll-pressed sheet, a filtrated buckypaper, and a spray-coated film. The roll-pressed sheet was made by simply roll-pressing a SWNT forest. The filtrated buckypaper was made from vacuum filtration of a sonicated SWNT dispersion in ethanol. The spray-coated film was made by spraying this same dispersion onto a surface and allowing it to dry without filtration. Emissivities of these samples (Fig. 5) were 0.62–0.76 (both for the sheet and buckypaper), 0.92 (spray-coat), being

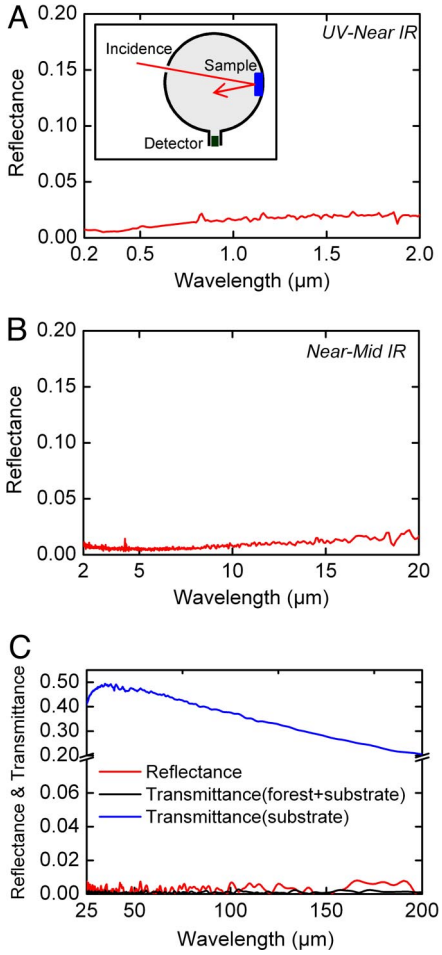

Fig. 4. Reflectance and transmittance spectra of SWNT forest. (*A*) Reflectance in the UV-to-near IR region (spectral range of 0.2–2.0 μm). The *Inset* illustrates the configuration of the reflectance measurements in the UV-to-near IR and the mid-to-far IR regions. (*B*) Reflectance in the near-to-mid IR region (2–20 μm). (*C*) Reflectance in the mid-to-far IR region (25–200 μm, red line) and transmittance of the substrate (black) and forest + substrate (blue).

distinctly lower than the 0.98 for the nanotube forest. These results are evidence that the black body behavior is not an intrinsic nanotube property but stems from the unique forest structure.

Fundamental optics shows that the black body behavior of the forest originates from its sparseness and alignment. A SWNT forest resembles an aerogel of vertically aligned SWNTs that

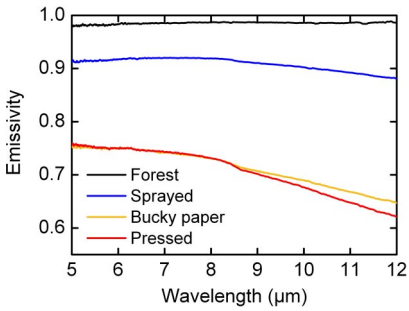

Fig. 5. Normal spectral emissivity of several SWNT structures. SWNT forest (black line), spray-coated film (blue), filtrated buckypaper (yellow), and roll-pressed sheet (red).

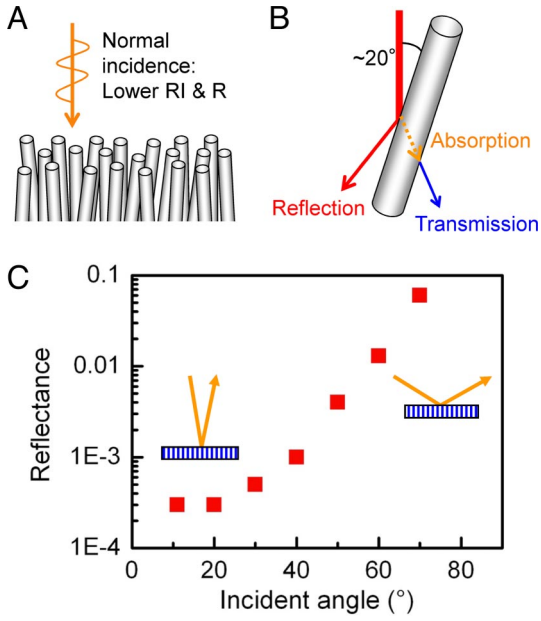

Fig. 6. Relationship between incident light and SWNT forest. (*A* and *B*) Schematic diagrams illustrating the interaction between incident light and SWNT forest (*A*) and individual SWNT (*B*). RI and R denote refractive index and reflectance, respectively. (*C*) Specular reflectance as a function of incident angle. Measurement with nonpolarized light with the wavelength ≈5 μm.

represent only 3% (97% air) of the total volume meaning that, on average, a 15 × 15-nm area is occupied by a single nanotube (19). It can be shown by fundamental optics that sparseness suppresses reflection. As described by Fresnel's law, normally incident light from an air medium (refractive index $n_0 = 1.0003$) onto a surface of refractive index, n, reflects with the reflectance

$$R = (n - n_0)^2/(n + n_0)^2. \quad [1]$$

This equation states that the reflection is suppressed when the refractive index of an object is close to that of air. However, for most solid materials, it is difficult to achieve low reflectance <0.02–0.03 because the refractive indices typically are >1.4 (e.g., MgF_2 1.38, fluorocarbon polymers 1.3–1.4), which corresponds to reflectance >0.028 from Eq. **1**. Importantly, this limit can be overcome by lowering the material density (increasing sparseness) thereby decreasing the electron density and therefore permissivity. Because the permissivity is proportional to the square of the refractive index, a decrease in permissivity results in a decrease of the refractive index, and thus a drop in reflectance (Fresnel's law).

Significantly, despite being a very sparse material, the forest appears as a homogeneous media, as viewed by the incident light. This is because the top surface is flat and uniform without microscale corrugations, and the largest observable structures are the interstitial regions separating SWNTs bundles being much smaller than the wavelength (Fig. 2*D*). The size distribution of the interstitial regions were estimated by liquid N_2 isotherms to be in the range of 5–30 nm, and this matches well with the size observed directly by high-resolution SEM images (Fig. 2*D* and theory). This homogeneous sparseness of the forest is one of the essential keys for achieving the low reflectance and high emissivity.

In addition to homogeneous sparseness, alignment also plays a critical role in achieving black body behavior. SWNTs within the forest are vertically aligned perpendicular to the substrate, with a tilt angle of ≈20° as shown by SEM images. As shown in the schematic (Fig. 6*A*), the forest structure can be thought of as

a sparse array of nanotube antennae. For an individual nanotube antenna, the interaction between a nanotube and light incident parallel to the tube axis is very weak, because in this direction the electrons cannot couple with the electric field. This leads to weak optical interaction between the forest and normally incident light, as evidenced by an experimentally observed 5-times drop in the absorbance for normal compared with parallel incident light (20). Similarly, normal incidence to the top of a forest results in low reflection and high transmission at the interface. Consequently, the majority of the light proceeds into the forest and interacts with the imperfectly aligned nanotubes (Fig. 6*B*). By each interaction, light is reflected, transmitted, or absorbed. Because SWNTs are good absorbers over the UV-to-far-infrared region (21, 22) and the tilt angle is small, back reflection is unlikely, and as the light propagates further into the body, it is quickly absorbed by the SWNTs. This interaction repeats until the attenuated light is completely absorbed by the forest. Although this applies to normal incidence, experiments show that reflectance remains low for nonnormal incident angles. The specular reflectance of a forest was examined over a variety of incident angles (11–70°) with a spectral range of 2–10 μm by using a FT-IR spectrometer equipped with a geminated ellipsoid mirror system (23, 24) (Fig. 6*C*). Although the intensity of the specular reflectance increased with incident angle, it remained considerably $<2\%$, which suggests that the argument holds for a wide range of incident angles. It should be noted that the observed specular reflectance (0.03% at 5 μm) is much smaller than the hemispherical reflectance (0.7% at 5 μm), and thus the specular dependence only provides an upper bound to the emissivity. Therefore, fundamentally, the homogeneous sparseness and aligned structure is critical for the SWNT forest to show black body behavior.

Conclusions

In conclusion, we have shown that the emissivity was 0.98–0.99 over a spectral range of 5–12 μm and the reflectance was 0.01–0.02 over a 0.2- to 200-μm range. These results highlight that a vertically aligned SWNT forest is a material most similar to a black body. This black body behavior originates from the unique structure of the forest as an assembly of nanotubes both sparsely distributed and vertically aligned.

Methods

Synthesis of SWNT Forest. Vertically aligned SWNTs (forests) were synthesized by water-assisted CVD ''SuperGrowth'' on silicon substrates at 750 °C with ethylene as a carbon source and water as a catalyst enhancer and preserver (25).

Emissivity Analysis. Normal spectral emissivity was evaluated in a home-built FT-IR spectrometer equipped with a Michelson interferometer and a photovoltaic HgCdTe detector at the National Metrology Institute of Japan (12, 26). All optical components, the SWNT forest sample, and 2 reference black body furnaces (set at −20 °C and 100 °C) were placed in vacuum to reduce absorption by air, and the estimated standard relative uncertainty was $<1\%$.

Reflectance and Transmittance Analyses. Optical reflectance of the SWNT forests was evaluated by 3 independent optical systems [see also Table S1]. For the UV-to-near IR (0.2–2 μm)/near-to-mid IR (2–20 μm) spectral ranges, a forest sample was set at the inner periphery of an integrating sphere (Fig. 4*A Inset*), and the light was incident near-normal to the sample with grating monochromator/FT-IR. The reflected light was collected by a detector with the integrating sphere (i.e., hemispherical-directional reflection) and subsequently normalized to a white reflectance standard (Spectralon)/gold mirror reference sample. For the mid-to-far IR region (25–200 μm), the specular reflectance and transmittance of a forest sample was evaluated by a FT-IR spectrometer and normalized to an aluminum mirror reference sample.

ACKNOWLEDGMENTS. We thank H. Shitomi and E. Kawate of the National Metrology Institute of Japan, Tokyo Metropolitan Industrial Technology Research Institute, and JASCO Corp. for reflectance analyses and J. Goto and J. Sato for technical assistance.

1. Serway RA (1986) *Physics for Scientists and Engineers with Modern Physics* (Saunders College Publishing, Philadelphia), 2nd Ed.
2. Nunes C, et al. (2002) Deposition of PVD solar absorber coatings for high-efficiency thermal collectors. *Vacuum* 67:623–627.
3. Cao A, Zhang X, Xu X, Wei B, Wu D (2002) Tandem structure of aligned carbon nanotubes on Au and its solar thermlal absorption. *Sol Energy Mater Sol Cells* 70:481–486.
4. Lira-Cantu M, Sabio AM, Brustenga A, Gomez-Romero P (2005) Electrochemical depositon of black nickel solar absorber coatings on stainless steel AISI316L for thermal solar cells. *Sol Energy Mater Sol Cells* 87:685–694.
5. Shashikala AR, Sharma AK, Bhandari DR (2007) Solar selective black nickel-cobalt coatings on aluminum alloys. *Sol Energy Mater Sol Cells* 91:629–635.
6. Lehman J, Theocharous E, Eppeldauer G, Pannell C (2003) Gold-black coatings for freestanding pyroelectric detectors. *Meas Sci Tech* 14:916–922.
7. Theocharous E, Deshpande R, Dillon AC, Lehman J (2006) Evaluation of a pyroelectric detector with a carbon multiwalled nanotube black coating in the infrared. *Appl Opt* 45:1093–1097.
8. Mellouki I, Bennaji N, Yacoubi N (2007) IR characterization of graphite black-coating for cryogenic detectors. *Infrared Phys Tech* 50:58–62.
9. Granqvist CG (1981) Radiative heating and cooling with spectrally selective surfaces. *Appl Opt* 20:2606–2615.
10. Kodama S, Horiuchi M, Kunii T, Kuroda K (1990) Ultra-black nickel-phosphorus alloy optical absorber. *IEEE Trans Inst Meas* 39:230–232.
11. Brown RJC, Brewer PJ, Milton MJT (2002) The physical and chemical properties of electroless nickel-phosphorus alloys and low reflectance nickel-phosphorus black surfaces. *J Mater Chem* 12:2749–2754.
12. Ishii J, Ono A (2003) A Fourier-transform spectrometer for accurate thermometric applications at low temperatures. *AIP Conference Proceeding 684 Temperature: Its Measurement and Control in Science and Industry* 7:705–710.
13. Taft EA, Philipp HR (1965) Optical properties of graphite. *Phys Rev* 138:A197–A202.
14. Touloukian YS (1970) *Thermophysical Properties of Matter, the TPRC Data Series* (IFI/Plenum, New York), Vol 8.
15. Xi J-Q, et al. (2007) Optical thin-film materials with low refractive index for broadband elimination of Fresnel reflection. *Nat Photon* 1:176–179.
16. Gershow M, Golovchenko JA (2007) Recapturing and trapping single molecules with a solid-state nanopore. *Nat Nanotechnol* 2:775–779.
17. Lee C, Bae SY, Mobasser S, Manohara H (2005) A novel silicon nanotips antireflection surface for the micro sun sensor. *Nano Lett* 5:2438–2442.
18. Yang Z-P, et al. (2008) Experimental observation of an extremely dark material made by a low-density nanotube array. *Nano Lett* 8:446–451.
19. Futaba DN, et al. (2006) 84% catalyst activity of water-assisted growth of single walled carbon nanotube forest characterization by a statistical and macroscopic approach. *J Phys Chem B* 110:8035–8038.
20. Murakami Y, Einarsson E, Edamura T, Maruyama S (2005) Polarization dependence of the optical absorption of single-walled carbon nanotubes. *Phys Rev Lett* 94:087402.
21. Itkis ME, et al. (2002) Spectroscopic study of the Fermi level electronic structure of single-walled carbon nanotubes. *Nano Lett* 2:155–159.
22. Itkis ME, Borondics F, Yu A, Haddon RC (2006) Bolometric infrared photoresponse of suspended single-walled carbon nanotube films. *Science* 312:413–416.
23. Kawate E (2005) Comparison of reflection methods for determining optical constants with STAR GEM. *Meas Sci Rev* 5:1–5.
24. Kawate E, Tesar R, Hain M (2007) New optical measurements realized by oblique incidence. *Meas Sci Rev* 7:63–66.
25. Hata K, et al. (2004) Water-assisted highly efficient synthesis of impurity-free single-walled carbon nanotubes. *Science* 306:1362–1364.
26. Ishii J, Ono A (2001) Uncertainty estimation for emissivity measurements near room temperature with a Fourier transform spectrometer. *Meas Sci Technol* 12:2103–2112.